Supernova Relic Electron Neutrinos and anti-Neutrinos in future Large-scale Observatories

C. Volpe* and J. Welzel†
Institut de Physique Nucléaire, F-91406 Orsay cedex, France
(Dated: February 2, 2008)

We investigate the signal from supernova relic neutrinos in future large scale observatories, such as MEMPHYS (UNO, Hyper-K), LENA and GLACIER, at present under study. We discuss that complementary information might be gained from the observation of supernova relic electron anti-neutrinos and neutrinos using the scattering on protons on one hand, and on nuclei such as oxygen, carbon or argon on the other hand. When determining the relic neutrino fluxes we also include, for the first time, the coupling of the neutrino magnetic moment to magnetic fields within the core-collapse supernova. We present numerical results on both the relic ν_e and $\bar{\nu}_e$ fluxes and on the number of events for ν_e+^{12}C, ν_e+^{16}O, ν_e+^{40}Ar and $\bar{\nu}_e$+p for various oscillation scenarios. The observation of supernova relic neutrinos might provide us with unique information on core-collapse supernova explosions, on the star formation history and on neutrino properties, that still remain unknown.

PACS numbers:
Keywords: core-collapse supernovae, supernova relic neutrinos, neutrino magnetic moment, resonant spin-flavour precession

arXiv:0711.3237v1 [astro-ph] 20 Nov 2007

I. INTRODUCTION

The observation of neutrinos from past core-collapse supernovae would represent an exciting and important discovery. Supernova relic neutrinos (SRN) bring crucial information on the explosion phenomenon, on the star formation rate and on neutrino properties. The understanding of how massive stars explode constitutes one of the main future challenges in astrophysics. While the various stages of the stellar evolution are quite well established, it still remains a mistery how, in these stars, the shock wave formed in the iron core, after collapse, manages to eject the mantle. Essentially all the gravitational energy is emitted in a short burst of neutrinos of all flavours. This luminosity curve follows closely the collapse, accretion phase and the cooling of the proto-neutron star left [1].

The first time such neutrinos have been observed is from the SN1987A located in the Large Magellanic Cloud, thanks to the IMB [2], Baksan [3] and Kamiokande detectors [4]. The few electron anti-neutrino events measured have roughly confirmed the theoretical expectations, even though their energy and angular distributions still have unsolved problems. For the SRN fluxes, the best upper limits at 90 % C.L. of 6.8 $\times$ 10^3 ν_e cm^{-2}s^{-1} (25 MeV $< E_{\nu_e} <$ 50 MeV) and 1.2 $\bar{\nu}_e$ cm^{-2}s^{-1} ($E_{\bar{\nu}_e} >$ 19.3 MeV) come from the LSD [5] and the Super-Kamiokande detectors [6]. The latter appears extremely close to most of theoretical predictions. Indeed it seems quite likely that the supernova relic neutrino background could be observed either by using an improved technology, e.g. the use of Gadolinium doped water Čerenkov detectors [7], or by scaling the present technology at megaton sizes, like in MEMPHYS [8], UNO [9], and Hyper-K [10]. These large-size observatories could provide us with the complementary information from a possible future (extra-)galactic explosion and from the SRN background.

Many authors have estimated the expected SRN flux using different approaches to determine the supernova rate [11, 12, 13, 14, 15, 16, 17] (see [18] for a review). In fact, the latter can be deduced either from direct observations [19] or from star formation rates (see e.g. [20]). The effects of neutrino masses and mixings on the SRN flux have been included recently (see e.g. [21]), [22]). In [23] a pragmatic approach has been used: to predict the SRN flux using available data, namely direct supernova rate measurements and supernova neutrino fluxes that give the best fit of the SN1987A events. Most of the available literature presents calculations for the $\bar{\nu}_e$ scattering on protons, which is the dominant detection channel in water Čerenkov (see e.g. [24]) or scintillator detectors [17]. In particular, a study of what could be learned on the neutrino spectra and/or the core-collapse supernova rate at next generation water Čerenkov detectors is realized in [25]. In Ref. [26] the potential of liquid argon detectors to observe supernova relic electron neutrinos is analyzed, while the specific case of ν_e detection in SNO is considered in [27, 28]. Ref. [28] also obtains an upper limit on the relic ν_e flux from the $\bar{\nu}_e$ upper limit in Super-Kamiokande. Finally, in [29, 30]

*Electronic address: volpe@ipno.in2p3.fr
†Electronic address: welzel@ipno.in2p3.fr

the authors have considered the possibility of using the SRN to gather information on more exotic unknown neutrino properties such as neutrino decay.

The study presented in this paper has several new features compared to the available literature. First we study the possible signal from both the supernova relic ν_e and $\bar{\nu}_e$ in future large-scale observatories. We consider the three technologies under investigation, water Čerenkov, scintillators and liquid argon, having in mind the proposed MEMPHYS (UNO, Hyper-K), LENA and GLACIER detectors [31]. We also include for the first time in the neutrino propagation within the supernova the interaction with matter (the Mikheev-Smirnov-Wolfenstein effect [32, 33]) as well as the coupling of the neutrino magnetic moment to the magnetic fields (the spin-flavour conversion phenomenon). Clearly our present understanding of supernovae explosion is still limited from several respects and, in particular, for the knowledge of the stellar magnetic fields and their evolution during the explosion. We think however that, even at the present stage, it is interesting to perform a first calculation including this process, to start investigating under which conditions some effects might be seen. We make here the assumption of a static supernova density profile, neglecting in this first work the changes induced by the shock wave. We also do not consider earth matter effects that have been discussed in [22]. To determine the SRN flux, we integrate the neutrino spectra from one supernova explosion over the redshift by convoluting it with the supernova explosion rate. We predict the expected event rates and analyse the effects of the presence of a neutrino magnetic moment both on the relic number fluxes and on the number of events. Note that we follow previous investigations for the choice of the neutrino fluxes at the neutrinosphere, of the supernova rate as well as for the discussion of the possible backgrounds in the detectors. The paper is organized as follows. The formalism is described in Section II. The results and conclusions are presented in Sections III and IV.

II. FORMALISM

A. Neutrino evolution in a core-collapse supernova with resonant spin-flavour conversion

Neutrino evolution including coupling with matter and with stellar magnetic fields (the resonant spin-flavour conversion or RSF) was first considered as a possible solution of the solar neutrino deficit problem [34, 35, 36]. We now know that this deficit is due to the presence of neutrino masses and mixings [37]. Even though the RSF might still give a sub-dominant contribution, it turns out to be extremely small [38]. The situation could be quite different in the case of massive stars such as core-collapse supernovae (SNII), since strong magnetic fields are expected, particularly close to the proto-neutron star surface. Many authors have investigated the RSF effects in SNII (see e.g. [39, 40, 41, 42, 43]).

The knowledge of the neutrino magnetic moment offers a serious challenge[1]. While the minimal extension of the Standard Model predicts a very small value [1], the observation of a large value would clearly indicate new physics. Several bounds have been obtained so far. Direct upper limits come from neutrino-electron scattering using neutrinos from reactors [37, 44, 45, 46], the best value being $9. \times 10^{-11}\ \mu_B$ at 90% C.L. [46]. Based on the electroweak radiative corrections to the neutrino mass, a model-independent theoretical upper bound is derived in [47]. Important indirect limits are obtained from astrophysical observations such as red-giant cooling [48] the SN1987A [39], or Big-Bang nucleosynthesis [49]. One might hope to attain improved direct limits with running experiments at reactors, a very intense tritium source, low energy beta-beams [50] or future astrophysical observations.

The neutrino evolution equations for three flavours including the interaction with matter and the coupling to the magnetic fields is given by ($\hbar = c = 1$):

$$i\frac{d}{dr}\begin{pmatrix}\nu\\ \bar{\nu}\end{pmatrix} = \begin{pmatrix}H_0 & BM\\ -BM & \bar{H}_0\end{pmatrix}\begin{pmatrix}\nu\\ \bar{\nu}\end{pmatrix}, \tag{1}$$

where ν ($\bar{\nu}$) stand for the electron, muon and tau (anti-)neutrinos. The hamiltonian H_0 includes the neutrino mixing and interaction with matter:

$$H_0 = \frac{1}{2E_\nu}U\begin{pmatrix}0 & 0 & 0\\ 0 & \Delta m^2_{12} & 0\\ 0 & 0 & \Delta m^2_{13}\end{pmatrix}U^\dagger + \begin{pmatrix}V^e_{cc}+V_{nc} & 0 & 0\\ 0 & V^\mu_{cc}+V_{nc} & 0\\ 0 & 0 & V^\tau_{cc}+V_{nc}\end{pmatrix}, \tag{2}$$

where the first term corresponds to neutrino propagation in vacuum while the second includes V^i_{cc}, the potential due to the charged-current neutrino scattering with electrons and V_{nc}, the neutral-current neutrino scattering with nucleons.

[1] Note that since neutrinos are massive particles they certainly have a non-zero magnetic moment.

In Eq.(2) U stands for the Maki-Nakagawa-Sakata-Pontecorvo (MNSP) matrix relating the neutrino flavor and mass basis. For anti-neutrinos, $\bar{H}_0$ is similar to H_0 but with a minus sign in front of the second term. The off diagonal terms come from the neutrino interactions with the SNII magnetic field, $B(r)$ and M is the magnetic moment matrix. Here we consider the case of Majorana neutrinos for which M is

$$M = \begin{pmatrix} 0 & \mu_{e\mu} & \mu_{e\tau} \\ -\mu_{e\mu} & 0 & \mu_{\mu\tau} \\ -\mu_{e\tau} & -\mu_{\mu\tau} & 0 \end{pmatrix} \tag{3}$$

with μ_{ij} the transition magnetic moments. (In [43] we have shown that neutrino flux modifications of less than 1 % are induced by the contribution of the neutrino magnetic moment to the neutrino scattering with matter. Here we do not consider these contributions.) From the RSF point of view Eq.(1) the relevant quantity is the product BM. The observation of RSF effects from a future SNII explosion signal, or from supernova relic neutrinos, might provide us with further information on the value of μ_ν and/or the strength and profile of the magnetic fields in SNII.

Coupling with matter or with magnetic fields can induce important modifications to neutrino oscillations. While the former produce ν_e versus ν_μ and ν_τ, the latter can produce ν_e versus $\bar{\nu}_\mu$ and $\bar{\nu}_\tau$ resonant conversions. The MSW resonances are situated at two densities governed by $(\Delta m^2_{13}, \theta_{13})$ and $(\Delta m^2_{12}, \theta_{12})$ respectively. The first resonance is located at density of about 10^3 g/cm^3 (MSW-h), while the second one at about 1 g/cm^3 (MSW-l). The neutrino conversion at each resonance depends on its adiabaticity. While the MSW-l resonance is adiabatic for typical supernova density profiles, the adiabaticity of MSW-h depends on the still unknown mixing angle θ_{13} [51, 52]. Similarly, a resonant ν_i versus $\bar{\nu}_j$ conversion (and vice-versa) can take place due to the presence of the neutrino magnetic moment. Three supplementary resonances are present in this case, their adiabaticy depending on the strength of the magnetic fields (see e.g. [42] for a detailed discussion).

B. Core-collapse supernova neutrinos and the supernova rate

Core-collapse supernovae are one of the most explosive phenomenon in our Universe. When the iron core of a massive star reaches its Chandrasekhar limit, an increased gravitational pull due to a contraction is no longer counterbalanced by the increase in the thermal pressure. The iron core collapses until it reaches nuclear densities and becomes very stiff. A shock wave is formed that moves outward ejecting the stellar mantle. How such ejection takes place remains still an unknown issue. Convection or extra energy deposit by neutrinos might offer the clue to this longstanding problem. In fact, most of the energy produced by the explosion is taken away by a short burst of neutrinos of all flavours. Their luminosity curve follows closely the different phases of the explosion.

Two ingredients are crucial to predict the SRN differential flux, dF/dE_ν, i.e. the neutrino flux from one supernova and the supernova rate :

$$\frac{dF}{dE_\nu} = \int_0^{z_{max}} \mathcal{R}_{SN}(z, \Omega_\lambda, \Omega_m) \frac{dn_\nu((1+z)E_\nu)}{dE_\nu} (1+z) \frac{dt}{dz} dz \tag{4}$$

where $\mathcal{R}_{SN}(z, \Omega_\lambda, \Omega_m)$ is the supernova rate per comoving volume at redshift z (Ω_λ and Ω_m are cosmological parameters, $\Omega_\lambda + \Omega_m = 1$ in the standard ΛCDM model), z_{max} is the redshift at which star formation started and $dn_\nu/dE_\nu((1+z)E_\nu)$ is the energy spectrum of emitted neutrinos leaving the supernova [21].

The neutrino spectra dn_ν/dE_ν at the neutrinosphere are quite well approximated by Fermi-Dirac [1] or power-law distributions [53]. Electron (anti)neutrinos interact with matter via charged as well as neutral current, while muon and tau neutrinos via neutral current only. The matter being neutron-rich and the cross sections for anti-neutrinos weaker than for neutrinos, we expect the following neutrino hierarchy: $\langle E_{\nu_e} \rangle < \langle E_{\bar{\nu}_e} \rangle < \langle E_{\nu_x, \bar{\nu}_x} \rangle$ with $x = \mu, \tau$. Supernova simulations predict typical temperatures of 10-13 MeV, 13-16 MeV and 16-23 MeV depending on the microphysics [53]. To determine the dn_ν/dE_ν at the SNII surface, we solve the neutrino evolution Eqs.(1-3), where one of the important unknowns is the stellar magnetic field. Here we consider that its shape follows a power-law, as done e.g. in [40]

$$B(r) = B_0 \left(\frac{r_B}{r} \right)^n \tag{5}$$

where $n = 2$ or 3 and $r_B = 1.4 \times 10^8$cm, the iron-core surface.

By including dt/dz and using

$$\mathcal{R}_{SN}(z, \Omega_\lambda, \Omega_m) = (1+z)^{-3/2} \sqrt{(1+\Omega_m z)(1+z^2) - \Omega_\lambda (2z + z^2)} \mathcal{R}_{SN}(z) \tag{6}$$

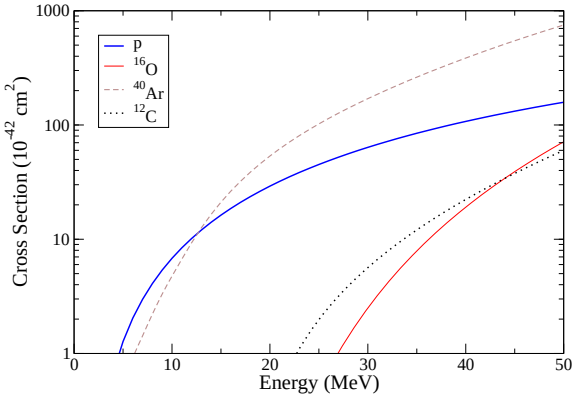


FIG. 1: Cross sections as a function of neutrino energy for $\bar{\nu}_e + p$ [54] and ν_e+^{12}C [55], ν_e+^{16}O [56] and ν_e+^{40}Ar [57].

one gets that dF/dE_ν is independent from the cosmological parameters:

$$dF/dE_\nu = \frac{1}{H_0}\int_0^{z_{max}} \mathcal{R}_{SN}(z)\frac{dn_\nu((1+z)E_\nu)}{dE_\nu}(1+z)^{-3/2}dz \tag{7}$$

where we take z_{max} equal to 4. For the supernova rate we consider the functional form from indirect observations accounting for the star formation rate [41]

$$\mathcal{R}_{SN}(z) = 1.22\times10^{-2}\times 0.3 f_\star h_{65}\frac{\exp(3.4z)}{\exp(3.8z)+45}\ \mathrm{yr}^{-1}\mathrm{Mpc}^{-3} \tag{8}$$

with $h_{65} = H_0/65\mathrm{km\ s}^{-1}\ \mathrm{Mpc}^{-1}$. The factor 1.22×10^{-2} is the fraction of SNII, deduced by assuming the Salpeter IMF (with a lower cutoff at 0.5 $M_\odot$ and taking all stars with $M > 8M_\odot$ as SNII). The normalization factor $f_\star$ takes into account the uncertainty on the local star formation rate density, which at $z = 0$ is (0.5-2.9)$\times10^{-2}h_{70}M_\odot$ year^{-1}Mpc^{-3}. The value $f_\star = 1$, that we will take in the following, is consistent with mildly dust-corrected UV data at low redshift [18] and predicts a local star formation rate of $0.7\times10^{-2}h_{70}M_\odot$ year^{-1}Mpc^{-3}. Note that according to [20], the local value for the star formation rate is $1.6\times10^{-2}h_{70}M_\odot$ year^{-1}Mpc^{-3} which means $f_\star = 2.5$. Here we do not perform a study of the sensitivity of the SRN flux to different choices of the $\mathcal{R}_{SN}(z)$ since this was performed in [21]. The different functionals available in the literature essentially have a very similar increasing behaviour for low redshifts ($z < 1$), well constrained by observations; while they might differ at high redshifts ($z > 1$). Note however that the latter contribute little to the signal in an observatory, if the detection threshold is larger than about 10 MeV.

Once the relic fluxes are obtained, the event rates are calculated by multiplying the SRN flux by the corresponding cross sections (Figure 1):

$$N_{events} = \int_{E_0} N_p dF/dE_\nu \sigma(E_\nu) dE_\nu \tag{9}$$

with E_0 the threshold energy that depends on the detector technology, N_p the number of target nucleons or nuclei, σ the relevant cross section.

III. RESULTS

We have calculated the neutrino evolution in a core-collapse supernova Eqs.(1-3) and then the relic supernova neutrino flux Eqs.(4-8). The oscillation parameters are fixed at $\Delta m^2_{12} = 8\times10^{-5}\mathrm{eV}^2$, $\sin^2 2\theta_{12} = 0.86$ and $\Delta m^2_{23} = 3\times10^{-3}\mathrm{eV}^2$, $\sin^2 2\theta_{23} = 0.96$ for the solar and atmospheric differences of the mass squares and mixings, respectively [37]. For the third still unknown neutrino mixing angle θ_{13}, we take either the present upper limit $\sin^2 2\theta_{13} = 0.19$ at 90 % C.L. (L) or a small value of $\sin^2 2\theta_{13} = 10^{-4}$ (S) that might be attained at the future (third generation) long-baseline

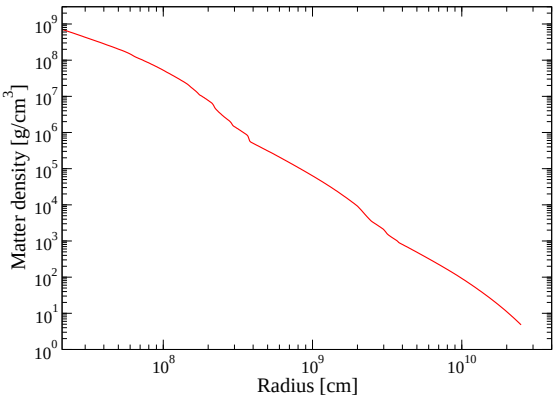


FIG. 2: Density profile of the pre-supernova progenitor used in this work [59].

experiments [58]. Since the sign of the atmospheric mixing is unknown, we consider both the normal (NH) and inverted (IH) hierarchy, i.e. $\Delta m^2_{13} > 0$ or < 0.

For the neutrino spectra at the neutrinosphere, we take Fermi-Dirac distributions as an example (Table I). We do not perform a detailed study of the sensitivity of the SRN flux predictions to different choices of the neutrino temperatures, from available supernova simulations, since this was done in [24]. The total luminosity is fixed at $L_0 = 3 \times 10^{53}$ ergs and the energy is assumed to be equally shared among all flavours (this is not necessarily true at early times). For the SNII matter density profile, we use a static 13.2 $M_\odot$ progenitor [59] (Figure 2). With the goal of also investigating the RSF effects on the SRN signal, we consider two different power law profiles Eq.(5) and the range of 0.001-1 values for the $\mu_{ij}B_0$ product Eqs.(1-3). These values correspond to taking at $r = r_B$ for example a magnetic field of $B_0 = 10^9$ ($B_0 = 10^{12}$) Gauss and a transition magnetic moment of 10^{-12} (10^{-15}) μ_B or $B_0 = 10^{12}$ Gauss and 10^{-12} μ_B respectively. In the following we will denote the largest value of 0.1 (1) for $n = 2$ ($n = 3$) by $(\mu B)_{large}$. Note that the radial profiles and the $\mu_{ij}B_0$ product are such that, while $\mu_{ij}B(r_B) = 0.1, 1$ for $n = 2, 3$; for both profiles $\mu_{ij}B(10r_B) = 0.001$ at the location of the RSF-h resonance. However, the behaviour is different at the RSF-l location. This has an impact on the expected rates, as we will see.

Electron fraction Y_e	T_{ν_e}	$T_{\bar{\nu}_e}$	$T_{\nu,\bar{\nu}_x}$	$\langle E_{\nu_e} \rangle$	$\langle E_{\bar{\nu}_e} \rangle$	$\langle E_{\nu,\bar{\nu}_x} \rangle$
0.48	3.5 MeV	5.1 MeV	7.0 MeV	11 MeV	16 MeV	22 MeV

TABLE I: Neutrino temperatures and average energies at the neutrinosphere.

A. The supernova relic ν_e and $\bar{\nu}_e$ fluxes

Figure 3 shows the neutrino spectra after propagation in the supernova for the two mass hierarchies and values of the third neutrino mixing angle (the magnetic fields or μ_ν are set to zero). The corresponding average neutrino energies are shown in Table II. Note that the value of θ_{13} determines the adiabaticity of the first MSW resonance at high density [51, 52], while θ_{12} governs the second (adiabatic) one at low density. As expected, when θ_{13} is large and the hierarchy is normal, maximal conversion occurs for electron neutrinos which acquire the hot spectrum of muon and tau neutrinos. On the other hand, for inverted hierarchy (when there is no resonance), the electron neutrino spectra are much colder. A similar behaviour is obtained for the electron anti-neutrinos, in the case of the inverted hierarchy.

The supernova relic ν_e and $\bar{\nu}_e$ fluxes, obtained after integrating over the redshift, are shown in Figures 4 to 6. The results including the RSF effects correspond to $\mu_{ij}B_0 = 0.1$ (1) for $n = 2$ ($n = 3$). We do not show the supernova

	NH-L		NH-S		IH-L		IH-S	
	$\langle E_{\nu_e}\rangle$	$\langle E_{\bar{\nu}_e}\rangle$	$\langle E_{\nu_e}\rangle$	$\langle E_{\bar{\nu}_e}\rangle$	$\langle E_{\nu_e}\rangle$	$\langle E_{\bar{\nu}_e}\rangle$	$\langle E_{\nu_e}\rangle$	$\langle E_{\bar{\nu}_e}\rangle$
MSW	21.5	17.7	18.8	17.4	17.9	21.8	17.6	18.5
$(\mu B)_{large}$ $n=2$	19.6	20.0	18.3	20.3	15.8	18.9	17.8	14.6
$(\mu B)_{large}$ $n=3$	19.3	21.4	18.2	21	21.5	14.2	19	16

TABLE II: Average energies (in MeV) of the ν_e and $\bar{\nu}_e$ fluxes, after the propagation in the SNII environment, with ($(\mu B)_{large}$ $n=2,3$) Eq.5 or without (MSW) the coupling to the magnetic fields. The different cases correspond to normal (NH) or inverted (IH) hierarchy and $\sin^2 2\theta_{13}=0.19$ (L) or $\sin^2 2\theta_{13}=10^{-4}$ (S).

	NH-L		NH-S		IH-L		IH-S	
	ν_e	$\bar{\nu}_e$	ν_e	$\bar{\nu}_e$	ν_e	$\bar{\nu}_e$	ν_e	$\bar{\nu}_e$
1 - 50 MeV	15.7	10.7	14.8	10.7	15.3	10.8	15.3	10.3
19.3 - 50 MeV	1.5	0.6	1.2	0.5	1.0	1.0	1.0	0.7
19.3 - 27 MeV	1.0	0.4	0.8	0.4	0.7	0.7	0.7	0.5

TABLE III: Relic Number Fluxes ($\mathrm{cm^{-2}s^{-1}}$) of electron neutrinos and anti-neutrinos, for different neutrino energy ranges and in the MSW case (no interaction with the magnetic field is included). The different cases correspond to normal (NH) or inverted (IH) hierarchy and $\sin^2 2\theta_{13}=0.19$ (L) or $\sin^2 2\theta_{13}=10^{-4}$ (S).

relic number fluxes obtained for values smaller than 0.001 (0.01) for $n=2$ ($n=3$) since the RSF effects are small and the results are close to the MSW solutions. For values within 0.001 (0.01) and 0.1 (1.) for $n=2$ ($n=3$) the results are in between the RSF and MSW ones. Table III presents the relic ν_e and $\bar{\nu}_e$ number fluxes integrated over different energy intervals. One can see that the relic ν_e number flux is larger than the $\bar{\nu}_e$ one in practically all cases[2]. Since the relic number fluxes are all peaked in the first 10 MeV, it is clear that this gives the most important contribution to the fluxes. Therefore detector energy thresholds around 10 or 20 MeV – as considered or used for example for LENA and water Čerenkov detectors respectively – are only sensitive to the tails of the SRN spectra. In the energy interval larger than 19.3 MeV, our $\bar{\nu}_e$ relic flux ranges between 0.4-0.7 $\mathrm{cm^{-2}s^{-1}}$, depending on the neutrino unknown parameters, and is compatible with the Super-Kamiokande limit of 1.2 $\mathrm{cm^{-2}s^{-1}}$ [6]. As far as the comparison to previous calculations is concerned, our predictions agree well with e.g. [21],[15].

B. Events in future observatories

We consider both the electron anti-neutrino signal associated to scattering on protons and the electron neutrino signal due to neutrino capture on nuclei. We take oxygen, carbon and argon as nuclear targets, having in mind the MEMPHYS (UNO, Hyper-K), LENA and GLACIER detectors at present under study [31]. The reactions of interest are[3]: $\bar{\nu}_e + p \rightarrow n + e^+$ and ν_e+^{16}O$\rightarrow e^-$+X or ν_e+^{12}C$\rightarrow e^-$+^{12}N for the water and scintillator detectors respectively; ν_e+^{40}Ar$\rightarrow e^-$+^{40}K for liquid argon. While the events associated to ^{16}O cannot be distinguished from the ones on protons in water Čerenkov detectors, those corresponding to ^{12}C can be identified by performing a double coincidence with the electrons from ^{12}N beta decay. It is clear that the both $\bar{\nu}_e + p \rightarrow n + e^+$ and the ν_e+^{40}Ar cross sections have the advantage of having a very low threshold and of being much larger compared to nuclear targets such as ^{12}C and ^{16}O (Figure 1). It is however important to emphasize that while the neutrino-proton cross section is known with high accuracy, this is not the case for neutrino-nucleus interactions. One might hope that by the time large-scale observatories are in operation, new facilities producing neutrinos in the 100 MeV energy range such as low energy beta-beams [60] or those based on conventional sources [61] might provide us with precise neutrino-nucleus cross sections.

Figures 7-8, 9-10 and 11-12 present the event rates for scattering of $\bar{\nu}_e$ on protons and ν_e on oxygen and argon,

[2] Note that our relic ν_e fluxes are compatible with the theoretical upper limit of 5.5 $\mathrm{cm^{-2}s^{-1}}$ extrapolated from the Super-Kamiokande result [28].

[3] Note that we do not consider here events produced by the $\bar{\nu}_e$+^{12}C$\rightarrow e^+$+^{12}B reaction in LENA, since the cross section and the $\bar{\nu}_e$ flux are smaller than in the ν_e case. For GLACIER, we do not consider other channels since the charged-current ν_e is the dominating one.

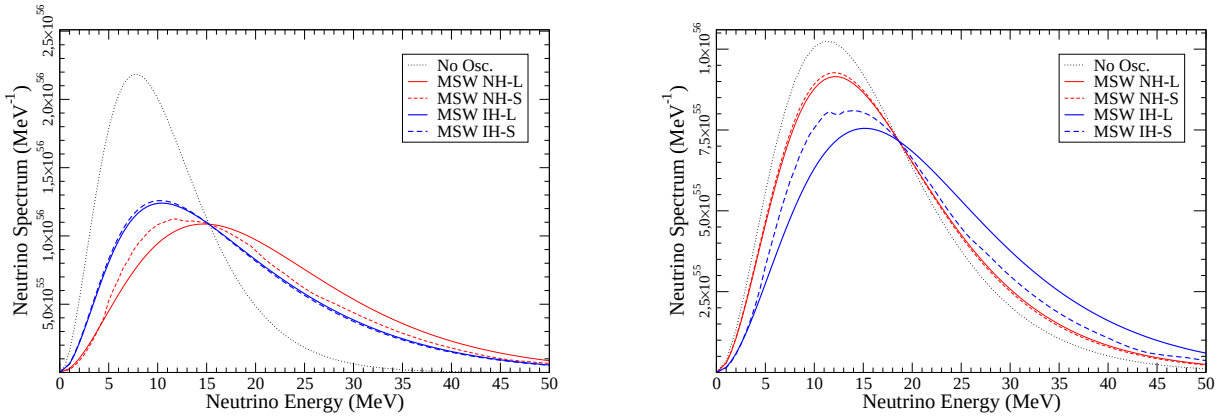


FIG. 3: Electron neutrino (left) and anti-neutrino (right) spectra after propagation in a core-collapse supernova, Eqs. (1-2) with $B = 0$, for the normal hierarchy with $\sin^2 2\theta_{13} = 0.19$ (NH-L) or $\sin^2 2\theta_{13} = 10^{-4}$ (NH-S) (thin solid and dashed lines) and the inverted hierarchy with $\sin^2 2\theta_{13} = 0.19$ (IH-L) or $\sin^2 2\theta_{13} = 10^{-4}$ (IH-S) (thick solid and dashed lines). The Fermi-Dirac distribution is also shown for comparison (dotted line).

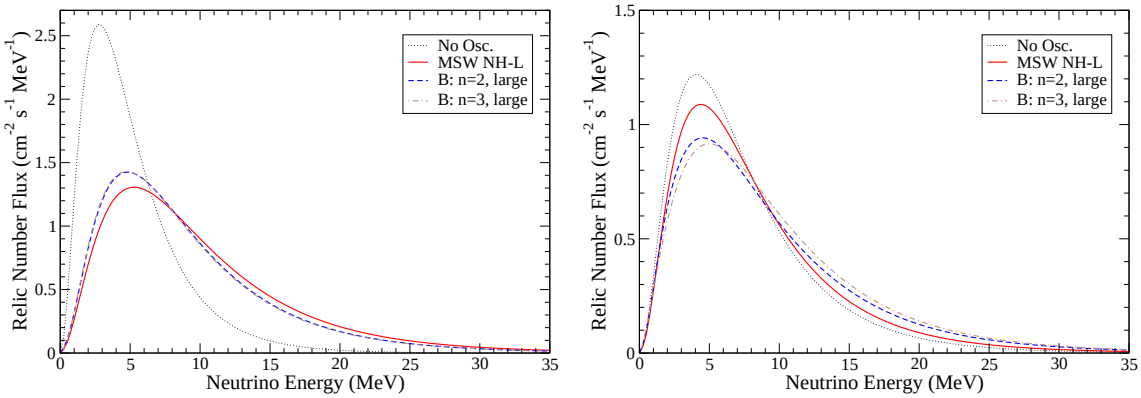


FIG. 4: Same as Fig. 3 but for the number flux of supernova relic neutrinos and anti-neutrinos Eqs.(1-8) with and without the coupling to the magnetic fields. Their radial profile is taken as a power law Eq.(5) with n=2,3 and the product $\mu_{ij}B$ is set to 1/0.1 for $n = 3/2$ (see text). For values much smaller than 0.01 (0.1) for $n = 2$ ($n = 3$) the results are close to the MSW solution and they are not shown. All curves correspond to the NH-L case. Similar results are obtained for the NH-S.

respectively. These curves can be easily understood from the the relic number fluxes (Figs. 4 to 6) and the cross sections (Figure 1), since the neutrino-nucleon and neutrino-nucleus cross sections behave approximately like E_ν^2. The corresponding expected number of events for $\bar{\nu}_e$ and ν_e in 10 years are shown in Tables IV-V[4] and VI-VII for the water Čerenkov (MEMPHYS, UNO, Hyper-K), scintillator (LENA[5]) or liquid argon (GLACIER) technologies. The detector sizes are those considered in the corresponding proposals, namely 440 kton fiducial mass (3 shafts), 50 kton and 100 kton respectively [31]. Here we consider that each detector has 100 % efficiency.

Extensive discussions about possible backgrounds can be found in the literature. A detailed investigation is preformed in [21] for water Čerenkov, in [17] for scintillators and in [26] for liquid argon. This issue is clearly crucial for the observation of relic supernova neutrinos. Three are the main sources of the backgrounds: solar neutrinos,

[4] Note that the $\bar{\nu}_e$+p event rates presented here for LENA are obtained with $f_\star = 1$ while in [17] with $f_\star = 2.5$.
[5] LENA is composed by 20 % PXE and 80 % Dodecane. The number of protons in the fiducial volume is 2.9×10^{33}.

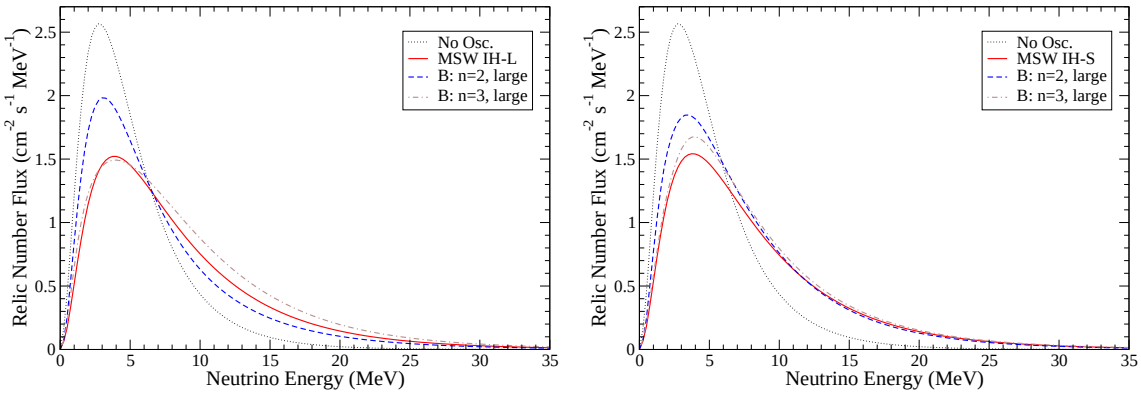


FIG. 5: Same as Fig. 4 but for electron neutrinos in the IH-L (left) and IH-S (right) cases.

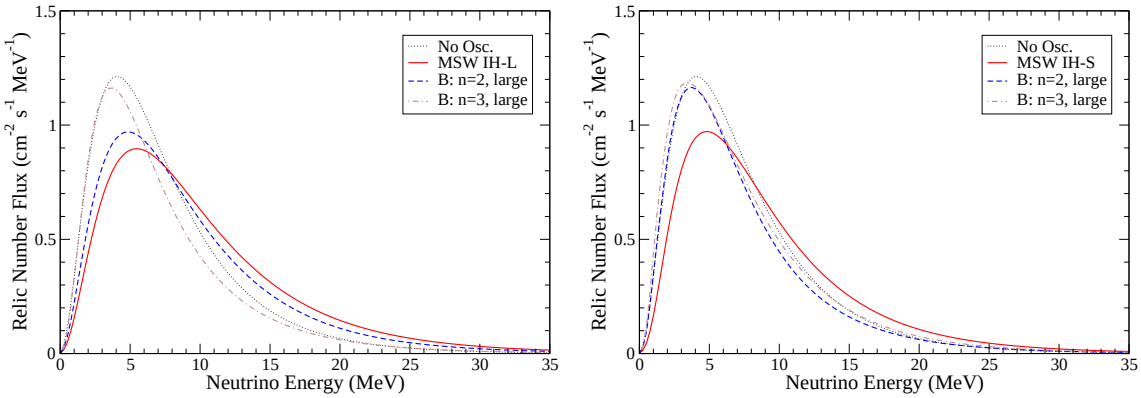


FIG. 6: Same as Fig. 5 but for electron anti-neutrinos.

reactor anti-neutrinos, atmospheric neutrinos. Solar neutrinos have low energies, the maximal being of almost 20 MeV coming from *hep*. Since water Čerenkov detectors do not have any charge identification, electron neutrinos can be mis-identified as anti-neutrinos. However, this background can be almost fully suppressed thanks to the good angular resolution of such detectors. On the other hand, the signal from electron neutrinos and anti-neutrinos can be distinguished in scintillator detectors. Concerning reactor electron anti-neutrinos, the flux is peaked at 2-3 MeV and has a tail reaching about 13 MeV. This contribution might be important or not depending on the chosen location. If present, it can clearly hinder SRN coming from $z \geq$1-2. In the case of the capture of the relic electron neutrinos by oxygen or carbon, the reaction threshold is so high that neither reactor nor solar neutrinos can produce a background. Atmospheric neutrinos produce events at higher energy. Note that in water Čerenkov detectors there is a supplementary source of background due to invisible muons. These are produced by atmospheric neutrinos that interact with the nucleons in the detector producing muons with energies below the Čerenkov radiation threshold. Figure 13 shows as an example the backgrounds in a scintillator detector such as LENA in comparison with our $\bar{\nu}_e$ rates.

Various authors have identified an energy window for the observation of relic supernova neutrinos, where the backgrounds are lower than the expected signal. At the present stage it might be premature to define an energy window for two reasons. First some backgrounds like for example the atmospheric one might scale differently in large-scale observatories from what is currently assumed. Secondly there are still many theoretical uncertainties coming either from supernova modelling, or from the knowledge of the supernova rate and from still unknown neutrino properties, in particular the knowledge of the hierarchy or of the θ_{13} value. For the above mentioned reasons we present the expected rates in two different energy windows. The 6.8 and 5-50 MeV energy ranges[6]are taken to show

[6] The threshold of 6.8 MeV takes into account the 1.8 MeV threshold energy for the reaction $\bar{\nu}_e$+p $\rightarrow$n + e$^+$ plus the 5 MeV necessary

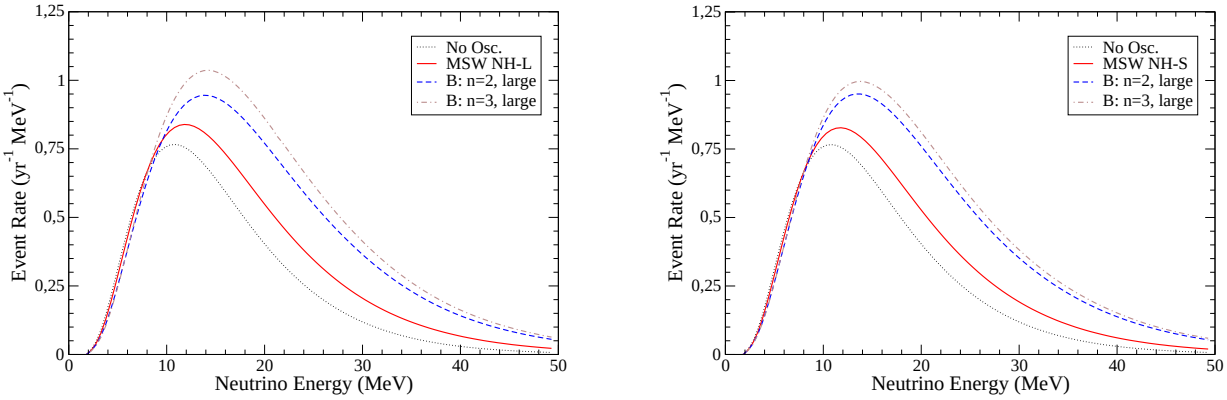


FIG. 7: Event rates (100 kton × year)$^{-1}$ for $\bar{\nu}_e + p \rightarrow n + e^+$ due to SRN for a normal hierachy and a large (left) or small (right) value of θ_{13}. The various curves present the results when the interaction with matter (MSW) and the coupling of the neutrino magnetic moment to the stellar magnetic fields are included (B large) with a radial dependence of r^{-2} (n=2) or r^{-3} (n=3) Eq.(5). The expected events when no oscillation is taken into account are shown for comparison.

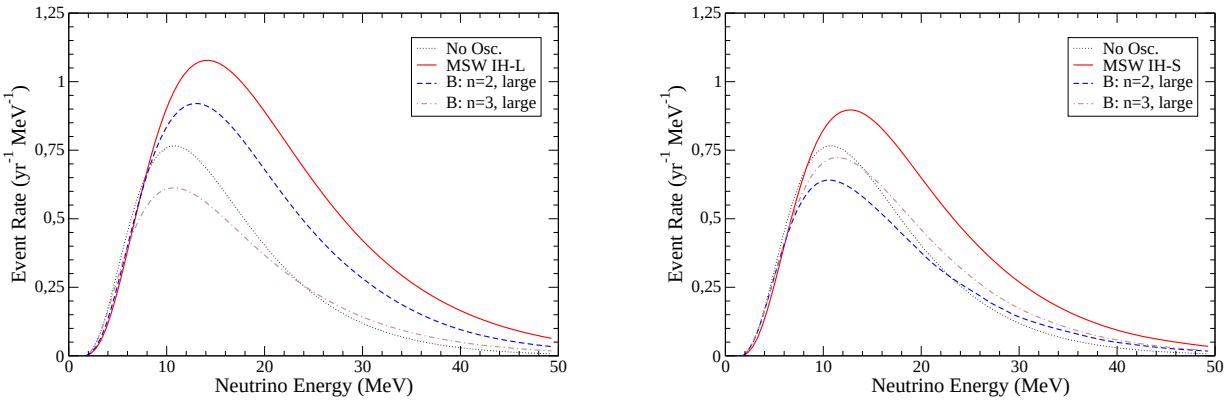


FIG. 8: Same as Figure 7 but for the inverted hierarchy.

how the event rate might increase if one manages to have a threshold as low as 6.8 and 5 MeV for the outgoing lepton and as high as 50 MeV, by suppressing the atmospheric background. Such an information, that might be helpful in the future, should be taken as indicative only. The 19.3-27, 9.3-25, 17.5-41.5 MeV for water Čerenkov, scintillators, liquid argon detectors are taken following Refs. [21],[17],[26] respectively. We make this choice to facilitate the comparison with available predictions[7].

As can be seen from Tables IV-V, in absence of the coupling to magnetic fields the largest number of events is expected for the IH-L case because of the MSW-h resonance. The events are larger by 50-60 %. In the normal hierarchy (θ_{13} large or small) case, electron anti-neutrinos undergoes regular matter effects and the RSF-h resonance

to observe the outgoing electron in water Čerenkov. The threshold of 5 MeV for scintillators is fixed in the same way.

[7] Note that our relic fluxes cross the backgrounds at higher energy (see for example 13). This would give energy ranges larger than the presented ones.

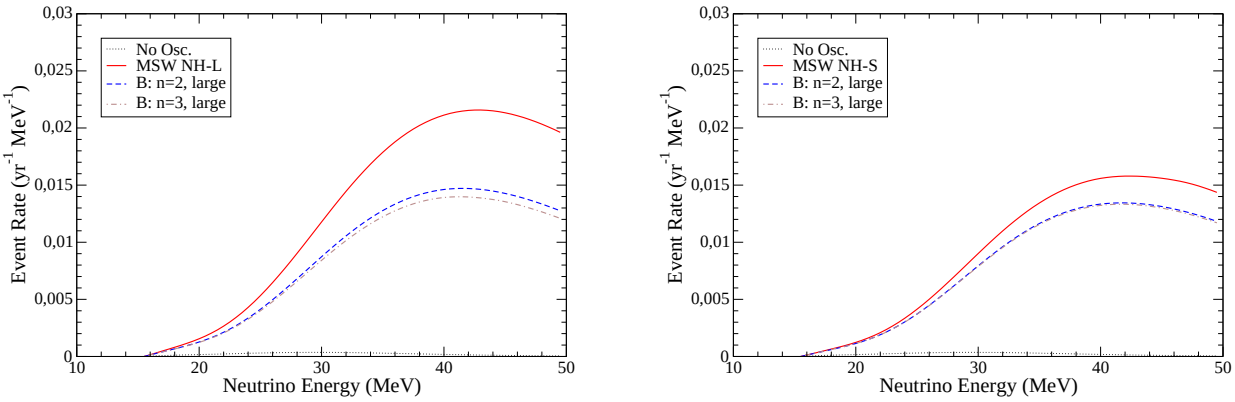


FIG. 9: Same as Figure 7 but for the event rates (100 kton $\times$ year)$^{-1}$ associated to ν_e+^{16}O$\rightarrow e^- + X$.

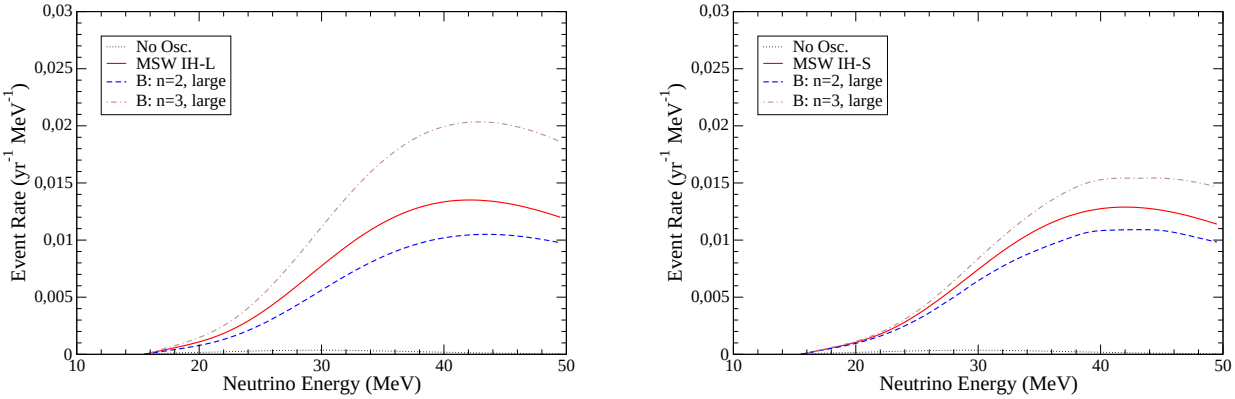


FIG. 10: Same as Figure 9 but for the inverted hierarchy.

which renders the electron anti-neutrinos hotter compared to the case with matters effects only. Therefore in presence of strong magnetic fields and/or large values of μ_{ij} the event rates can be increased by 30 to 50 %. For the inverted hierarchy, electron anti-neutrinos encounter both the MSW-h and the RSF-h resonances. In this case the events are significantly reduced. The two magnetic field profiles considered give similar results, except for the inverted hierarchy and large mixing angle. For this case and if the $n = 2$ profile is taken, the anti-neutrinos undergo the RSF-l resonance as well. As a consequence the number of events is doubled compared to the $n = 3$ profile and is close to the MSW result.

In Tables VI-VII we show the predicted events in the case of electron neutrino-nucleus scattering, choosing large intervals only[8], except for the argon case. In fact, this is the first time that interactions of SRN on oxygen and carbon are considered. Since a detailed study of the atmospheric backgrounds for these cases does not exist, we hope that our work will trigger investigations of this channels for MEMPHYS (UNO, Hyper-K) and LENA. A few events are found for ν_e+^{12}C, up to 20 for ν_e+^{16}O, and 100-200 for ν_e+^{40}Ar. Note that the large number of events found for ν_e+^{40}Ar

[8] The 20.5 MeV threshold includes the reaction threshold and 5 (3) MeV electron energy for MEMPHYS (LENA).

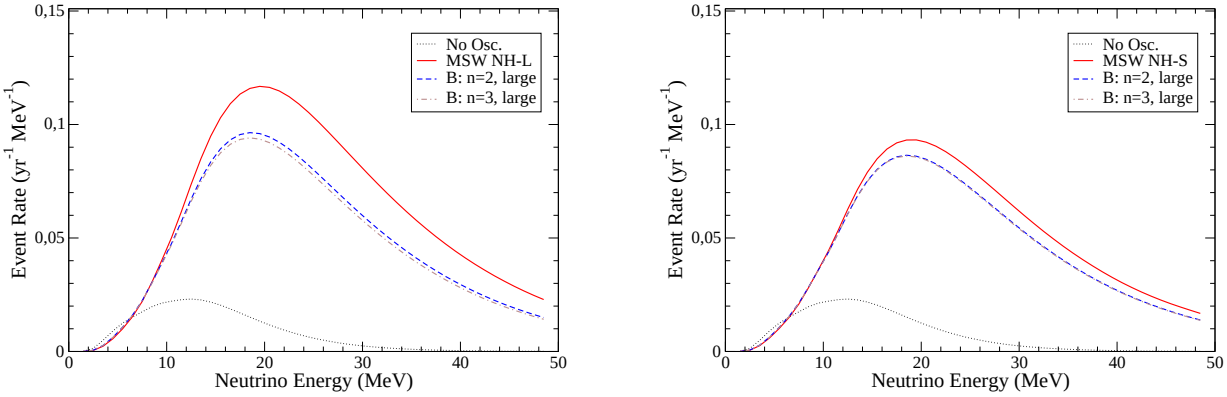


FIG. 11: Same as 7 but for the event rates (10 kton $\times$ year)$^{-1}$ associated to ν_e+^{40}Ar$\rightarrow$ e^-+^{40}K .

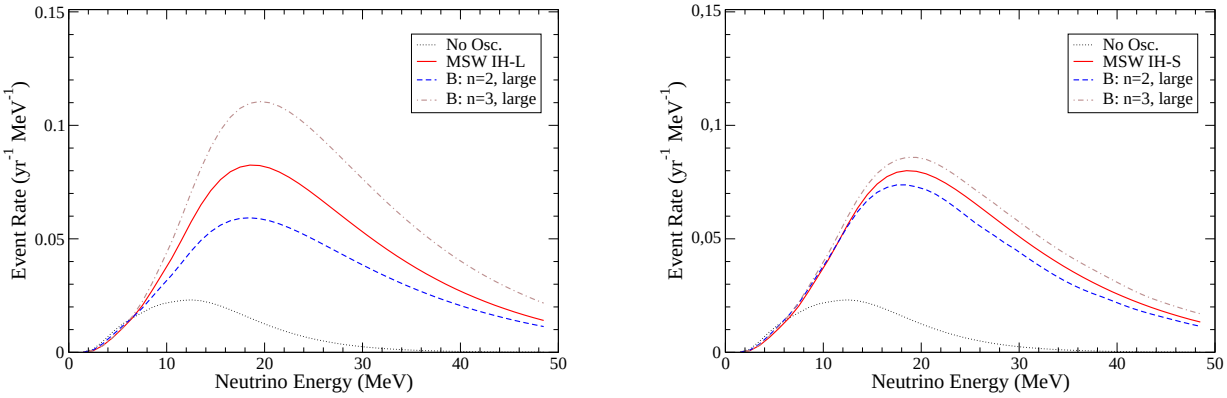


FIG. 12: Same as Figure 11 but for the inverted hierarchy.

is due both to the large cross section (Figure 1) and to the large ν_e flux (Table III). In absence of magnetic moment effects, the maximal conversion for electron neutrinos occurs for a normal hierarchy and a large θ_{13} value, due to the MSW-h resonance. In fact, since ν_e gets a hotter spectrum because of the mixing with ν_μ, ν_τ neutrinos the number of events is increased by 30-60 % compared to the case when the resonance is not (fully) adiabatic or of normal matter effects. On the other hand, RSF conversions from ν_e to $\bar{\nu}_\mu, \bar{\nu}_\tau$ generally decrease by 20-40 %, compared to the MSW only, in most cases. The only exception is for the inverted hierarchy and the $n = 3$ magnetic field profile for which the events increase by 15 up to 50 %. It is clear that the search for relic ν_e might either improve the present LSD limit [5] (in case of non-observation) or bring crucial information to our understanding of core-collapse supernova and neutrino physics.

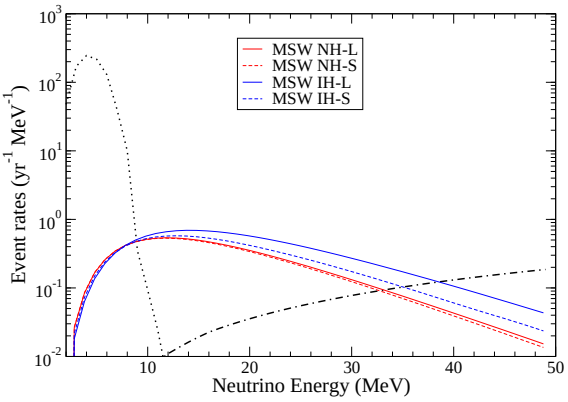


FIG. 13: Expected event rates in the LENA detector for normal (NH) and inverted (IH) hierarchy as well as a small (S) and a large (L) third neutrino mixing angle. Both the reactor electron anti-neutrinos (dotted line) at Pyhäsalmi and the atmospheric (dashed-dotted line) backgrounds are shown. The backgrounds are from Ref.[17, 62].

	MEMPHYS $\bar{\nu}_e$+p		LENA $\bar{\nu}_e$+p	
	6.8 - 50	19.3 - 27	5.0 - 50	9.3 - 25
MSW NH-L	652	142	67	44
$(\mu B)_{large}$ NH-L	873 (968)	214 (240)	89 (97)	55 (61)
MSW NH-S	631	135	65	43
$(\mu B)_{large}$ NH-S	868 (921)	209 (225)	88 (94)	55 (58)

TABLE IV: Expected number of events after 10 years for electron anti-neutrino scattering on protons in MEMPHYS (water Čerenkov) or LENA (scintillator) detectors. The size considered is 440 kton fiducial mass, 50 kton and 100 kton respectively, following the corresponding proposals [31]. An efficiency of 100 % is assumed. The calculations correspond to the normal hierarchy (NH) and large (L) or small (S) value of the third neutrino mixing angle. The calculations include the coupling of neutrinos to matter effects without (MSW) or with the coupling to the stellar magnetic fields ($(\mu B)_{large}$) . The stellar magnetic profile is taken to be a power-law Eq.(5) with $n = 2$ ($n = 3$ results are given in parenthesis). Two energy intervals are considered (see text).

	MEMPHYS $\bar{\nu}_e$+p		LENA $\bar{\nu}_e$+p	
	6.8 - 50	19.3 - 27	5.0-50	9.3-25
MSW IH-L	997	248	101	64
$(\mu B)_{large}$ IH-L	776 (464)	181 (95)	80 (48)	51 (30)
MSW IH-S	751	173	77	50
$(\mu B)_{large}$ IH-S	479 (559)	98 (120)	51 (58)	32 (38)

TABLE V: Same as Table IV but for the inverted hierarchy.

IV. CONCLUSIONS

In this work we have analysed both the relic supernova electron anti-neutrino and neutrino fluxes and the associated signals due to scattering on protons and nuclei respectively, in large-scale observatories such as MEMPHYS (UNO, Hyper-K), LENA or GLACIER. Our calculations of the neutrino propagation in the star include both the matter interaction and the resonant spin-flavour conversion. One of our goals has been to try to investigate under which conditions (profile, μ_{ij} and/or B_0 values) RSF effects could be seen. In all cases studied, the results show that RSF

	MEMPHYS	LENA	GLACIER	
	$\nu_e + {}^{16}$O	$\nu_e + {}^{12}$C	$\nu_e + {}^{40}$Ar	
Energy Range (MeV)	20.5 - 50	20.5 - 50	4.5 - 50	17.5-41.5
MSW NH-L	19	2.9	297	197
$(\mu B)_{large}$ NH-L	14 (13)	2.1 (2.0)	235 (228)	141(156)
MSW NH-S	14	2.2	235	152
$(\mu B)_{large}$ NH-S	12 (12)	2.0 (1.9)	213 (212)	136(135)

TABLE VI: Expected number of events after 10 years for electron neutrino scattering on nuclei in MEMPHYS (water Čerenkov), LENA (scintillator) or GLACIER (liquid argon) detectors. The size considered is 440 kton, 50 kton and 100 kton respectively, following the corresponding proposals [31]. An efficiency of 100 % is assumed. The calculations correspond to the normal hierarchy (NH) and large (L) or small (S) value of the third neutrino mixing angle. The calculations include the coupling of neutrinos to matter effects without (MSW) or with the coupling to the stellar magnetic fields ($(\mu B)_{large}$) . The stellar magnetic profile is taken to be a power-law Eq.(5) with $n = 2$ ($n = 3$ results are given in parenthesis). Two energy intervals are considered in the case of argon (see text).

	MEMPHYS	LENA	GLACIER	
	$\nu_e + {}^{16}$O	$\nu_e + {}^{12}$C	$\nu_e + {}^{40}$Ar	
Energy Range (MeV)	20.5 - 50	20.5 - 50	4.5 - 50	17.5-41.5
MSW IH-L	12	1.9	207	132
$(\mu B)_{large}$ IH-L	9 (18)	1.4 (2.8)	155 (282)	95 (186)
MSW IH-S	12	1.8	200	127
$(\mu B)_{large}$ IH-S	10 (14)	1.5 (2.1)	181 (221)	112(142)

TABLE VII: Same as Table VI but for the inverted hierarchy.

phenomenon might increase/decrease significantly the number of events, for strong magnetic fields and/or large values of the neutrino magnetic moment. It is interesting to note that these effects are maximal for electron anti-neutrinos, when no resonant conversion is present due to matter efffects (normal hierarchy and a large or small value of θ_{13}) due to the RSF-h resonance. In the case of electron neutrinos, the RSF tend to decrease the events, in most cases. Our results are also sensitive to the magnetic field profiles. To obtain thes results with the spin-flavour conversion, we have made the assumption of a static density supernova profile and also neglected possible effects of the shock wave on the stellar magnetic fields. Our present knowledge in this respect is in fact still too limited to include such aspects. From this point of view, our analysis should be taken as a first step in this direction and should be updated once progress is performed on the knowledge of the supernova magnetic fields and on the shock wave impact.

Our main goal has been to perform a numerical study of the relic fluxes and their signal in the next generation observatories. We have obtained that ν_e fluxes are larger than the $\bar{\nu}_e$ up to a factor 2.5 depending on the oscillation scenarios (normal or inverted hierarchy and θ_{13} value). We have shown that, after 10 years operation, between 100 and 250 $\bar{\nu}_e + p$ events are expected in the 19.3-27 MeV neutrino energy range for MEMPHYS, while 45-65 are expected in LENA in the 9.3-25 MeV energy range. We find that neutrino-carbon scattering will produce 2-3 events, while neutrino-oxygen will give 10-20 events and the neutrino-argon interaction will induce 100 to 200 events. (These number are obtained by taking the normalization factor for the star formation rate $f_\star = 1$, which implies a local formation rate of $0.7\times10^{-2}h_{70}M_\odot$ year^{-1}Mpc^{-3}, consistent with mildly dust-corrected UV data at low redshift). The possible measurement of both ν_e and $\bar{\nu}_e$ could help us determining the neutrino fluxes at the neutrinosphere and/or still unknown neutrino properties, such as the hierarchy or the knowledge of the third neutrino mixing angle. This will depend on the progress made in supernova modelling or neutrino physics by the time such observatories might come into operation. In conclusion, future large-scale observatories based on water, scintillator or liquid argon have a great discovery potential for relic supernova neutrinos. Their observation would clearly provide us with essential information on core-collapse supernova explosions, the supernova explosion rate and important neutrino properties that still remain unknown.

ACKNOWLEDGMENTS

We are grateful to Takashi Yoshida for illuminating discussions and to Shin'ichiro Ando, Gail McLaughlin, Jim Kneller, Karlheinz Langanke, Teresa Marrodan Undagoitia, Mauro Mezzetto, Alessandra Tonazzo, Petr Vogel, Michael Wurm for providing us with useful information. We acknowledge support from the project ANR-05-JC-JC0023 "Non-standard neutrino properties and their impact in astrophysics and cosmology" (NeuPAC).

[1] G. G. Raffelt, "Stars As Laboratories For Fundamental Physics: The Astrophysics Of Neutrinos, Axions, And Other Weakly Interacting Particles", Chicago, USA: Univ. Pr. (1996); and references therein.
[2] R.M. Bionta et al., Phys. Rev. Lett. **58** (1987) 1494.
[3] E.N. Alexeyev et al., JETP Lett. **45** (1987) 589.
[4] K.S. Hirata et al., Phys. Rev. Lett. **58** (1987) 1490.
[5] M. Aglietta *et al.*, Astropart. Phys. **1** (1992) 1.
[6] M. Malek *et al.* [Super-Kamiokande Collaboration], Phys. Rev. Lett. **90** (2003) 061101 [arXiv:hep-ex/0209028].
[7] J. F. Beacom and M. R. Vagins, Phys. Rev. Lett. **93**, 171101 (2004) [arXiv:hep-ph/0309300].
[8] A. de Bellefon *et al.*, arXiv:hep-ex/0607026.
[9] C.K. Jung, Proceedings of the Next generation Nucleon Decay and Neutrino Detector (NNN99) Workshop, September 23-25, 1999, Stony Brook, New York [hep-ex/0005046].
[10] Itow et al., hep-ex/0106019.
[11] R. A. Malaney, Astropart. Phys. **7** (1997) 125 [arXiv:astro-ph/9612012].
[12] D. H. Hartmann and S. E. Woosley, Astropart. Phys. **7** (1997) 137.
[13] T. Totani, K. Sato and Y. Yoshii, Astrophys. J. **460** (1996) 303 [arXiv:astro-ph/9509130].
[14] M. Kaplinghat, G. Steigman and T. P. Walker, Phys. Rev. D **62** (2000) 043001 [arXiv:astro-ph/9912391].
[15] L. E. Strigari, M. Kaplinghat, G. Steigman and T. P. Walker, JCAP **0403** (2004) 007 [arXiv:astro-ph/0312346].
[16] M. Fukugita and M. Kawasaki, Mon. Not. Roy. Astron. Soc. **340** (2003) L7 [arXiv:astro-ph/0204376].
[17] M. Wurm, F. von Feilitzsch, M. Goeger-Neff, K. A. Hochmuth, T. M. Undagoitia, L. Oberauer and W. Potzel, Phys. Rev. D **75** (2007) 023007 [arXiv:astro-ph/0701305].
[18] S. Ando and K. Sato, New J. Phys. **6** (2004) 170 [arXiv:astro-ph/0410061].
[19] E. Cappellaro, M. Turatto, D. Y. Tsvetkov, O. S. Bartunov, C. Pollas, R. Evans and M. Hamuy, Astron. Astrophys. **322** (1997) 431 [arXiv:astro-ph/9611191].
[20] L. E. Strigari, J. F. Beacom, T. P. Walker and P. Zhang, JCAP **0504**, 017 (2005) [arXiv:astro-ph/0502150].
[21] S. Ando, K. Sato and T. Totani, Astropart. Phys. **18** (2003) 307 [arXiv:astro-ph/0202450].
[22] S. Ando and K. Sato, Phys. Lett. B **559** (2003) 113 [arXiv:astro-ph/0210502].
[23] C. Lunardini, Astropart. Phys. **26** (2006) 190 [arXiv:astro-ph/0509233].
[24] S. Ando, Astrophys. J. **607** (2004) 20 [arXiv:astro-ph/0401531].
[25] C. Lunardini, Phys. Rev. D **75** (2007) 073022 [arXiv:astro-ph/0612701].
[26] A. G. Cocco, A. Ereditato, G. Fiorillo, G. Mangano and V. Pettorino, JCAP **0412**, 002 (2004) [arXiv:hep-ph/0408031].
[27] J. F. Beacom and L. E. Strigari, Phys. Rev. C **73** (2006) 035807 [arXiv:hep-ph/0508202].
[28] C. Lunardini, Phys. Rev. D **73** (2006) 083009 [arXiv:hep-ph/0601054].
[29] S. Ando, Phys. Lett. B **570** (2003) 11 [arXiv:hep-ph/0307169].
[30] G. L. Fogli, E. Lisi, A. Mirizzi and D. Montanino, Phys. Rev. D **70** (2004) 013001 [arXiv:hep-ph/0401227].
[31] D. Autiero *et al.*, arXiv:0705.0116 [hep-ph].
[32] L. Wolfenstein, Phys. Rev. D **17**, 2369 (1978).
[33] S. P. Mikheev and A. Y. Smirnov, Nuovo Cim. C **9**, 17 (1986).
[34] A. Cisneros, Astrophys. Space Sci. **10** (1971) 87.
[35] C. S. Lim and W. J. Marciano, Phys. Rev. D **37** (1988) 1368.
[36] E. K. Akhmedov, Phys. Lett. B **213**, 64 (1988).
[37] W. M. Yao *et al.* [Particle Data Group], J. Phys. G **33** (2006) 1.
[38] A. B. Balantekin and C. Volpe, Phys. Rev. D **72** (2005) 033008 [arXiv:hep-ph/0411148].
[39] J. M. Lattimer and J. Cooperstein, Phys. Rev. Lett. **61** (1988) 23.
[40] H. Nunokawa, Y. Z. Qian and G. M. Fuller, Phys. Rev. D **55** (1997) 3265 [arXiv:astro-ph/9610209].
[41] S. Ando and K. Sato, Phys. Rev. D **67** (2003) 023004 [arXiv:hep-ph/0211053].
[42] E. K. Akhmedov and T. Fukuyama, JCAP **0312**, 007 (2003) [arXiv:hep-ph/0310119].
[43] A. B. Balantekin, C. Volpe and J. Welzel, JCAP **0709** (2007) 016 [arXiv:0706.3023 [astro-ph]].
[44] F. Reines, H. S. Gurr and H. W. Sobel, Phys. Rev. Lett. **37** (1976) 315.
[45] H.B. Li, et al, TEXONO Collaboration, Phys. Rev. Lett. **90**, 131802 (2003).
[46] Z. Daraktchieva *et al.* [MUNU Collaboration], Phys. Lett. B **615** (2005) 153 [arXiv:hep-ex/0502037].
[47] N. F. Bell, M. Gorchtein, M. J. Ramsey-Musolf, P. Vogel and P. Wang, Phys. Lett. B **642**, 377 (2006) [arXiv:hep-ph/0606248].
[48] G. G. Raffelt, Phys. Rev. Lett. **64** (1990) 2856.

[49] J. A. Morgan, Phys. Lett. B **102**, 247 (1981).
[50] G. C. McLaughlin and C. Volpe, Phys. Lett. B **591** (2004) 229 [arXiv:hep-ph/0312156].
[51] A. S. Dighe and A. Y. Smirnov, Phys. Rev. D **62** (2000) 033007 [arXiv:hep-ph/9907423].
[52] J. Engel, G. C. McLaughlin and C. Volpe, Phys. Rev. D **67** (2003) 013005 [arXiv:hep-ph/0209267].
[53] M. T. Keil, G. G. Raffelt and H. T. Janka, Astrophys. J. **590** (2003) 971 [arXiv:astro-ph/0208035].
[54] A. B. Balantekin, J. H. de Jesus, R. Lazauskas and C. Volpe, Phys. Rev. D **73** (2006) 073011 [arXiv:hep-ph/0603078].
[55] C. Volpe, N. Auerbach, G. Colo, T. Suzuki and N. Van Giai, Phys. Rev. C **62** (2000) 015501 [arXiv:nucl-th/0001050].
[56] R. Lazauskas and C. Volpe, Nucl. Phys. A **792** (2007) 219 [arXiv:0704.2724 [nucl-th]].
[57] P. Vogel and K. Langanke, private communication.
[58] C. Volpe, J. Phys. G **34**, R1 (2007) [arXiv:hep-ph/0605033].
[59] J. P. Kneller, G. C. McLaughlin and J. Brockman, arXiv:0705.3835 [astro-ph].
[60] C. Volpe, J. Phys. G **30** (2004) L1 [arXiv:hep-ph/0303222].
[61] See http://www.phy.ornl.gov/nusns/ ; Y. Efremenko, Private communication.
[62] M. Wurm and T. Marrodan Undagoitia, Private communication.